J. Phys.: Condens. Matter 7 (1995) 9447–9464. Printed in the UK

Spin-dependent transport in metal/semiconductor tunnel junctions

M W J Prins†§, H van Kempen†, H van Leuken†, R A de Groot†, W Van Roy‡‖ and J De Boeck‡

† Research Institute for Materials, University of Nijmegen, Toernooiveld 1, NL-6525 ED Nijmegen, The Netherlands

‡ Imec, Kapeldreef 75, B-3001, Leuven, Belgium

Received 31 July 1995, in final form 16 October 1995

Abstract. This paper describes a model as well as experiments on spin-polarized tunnelling with the aid of optical spin orientation. This involves tunnel junctions between a magnetic material and gallium arsenide (GaAs), where the latter is optically excited with circularly polarized light in order to generate spin-polarized carriers. A transport model is presented that takes account of carrier capture in the semiconductor surface states, and describes the semiconductor surface in terms of a spin-dependent energy distribution function. The so-called surface spin-splitting can be calculated from the balance of the polarized electron and hole flow in the semiconductor subsurface region, the polarized tunnelling current across the tunnel barrier between the magnetic material and the semiconductor surface, and the spin relaxation at the semiconductor surface.

Measurements are presented of the circular-polarization-dependent photocurrent (the so-called helicity asymmetry) in thin-film tunnel junctions of $Co/Al_2O_3/GaAs$. In the absence of a tunnel barrier, the helicity asymmetry is caused by magneto-optical effects (magnetic circular dichroism). In the case where a tunnel barrier is present, the data cannot be explained by magneto-optical effects alone; the deviations provide evidence that spin-polarized tunnelling due to optical spin orientation occurs. In Co/τ-MnAl/AlAs/GaAs junctions no deviations from the magneto-optical effects are observed, most probably due to the weak spin polarization of τ-MnAl along the tunnelling direction; the latter is corroborated by bandstructure calculations. Finally, the application of photoexcited GaAs for spin-polarized tunnelling in a scanning tunnelling microscope is discussed.

1. Introduction

Since the early seventies, spin-polarized tunnelling studies have been conducted in order to derive information about spin-dependent electronic states [1]. These studies involved thin-film tunnel junctions as well as junctions in a scanning tunnelling microscope (STM) [2]. As the spin-selective probe material, there are essentially three possibilities: (i) a superconductor, (ii) a magnetic material, or (iii) a semiconductor. For each of these materials, in this introductory section we very briefly point out how spin selectivity can be achieved, and mention the experiments already performed with planar solid-state tunnel junctions as well as in an STM.

§ Present address: Philips Research Laboratories, Prof. Holstlaan 4, 5656 AA Eindhoven, The Netherlands.

‖ Present address: Joint Research Centre for Atom Technology (JRCAT), National Institute for Advanced Interdisciplinary Research (NAIR), 1-1-4 Higashi, Tsukuba, Ibaraki 305, Japan.

0953-8984/95/499447+18$19.50

(i) The measurement of spin-polarized tunnelling with a superconducting material is based on the Zeeman splitting of the (unpaired) quasiparticle states of a spin-paired superconductor (for an excellent review see [1]). As a result of an applied magnetic field H, in a small spectral range of order $\mu_B H$ at the edges of the superconducting gap, tunnelling with only one spin orientation is achieved. By measuring the differential conductance versus applied voltage, it is possible to determine the spin polarization of the tunnelling current. Many successful experiments were performed with thin-film tunnel junctions involving superconducting Al, an Al_2O_3 tunnel barrier, and a wide variety of magnetic counter-electrodes.

(ii) In the case of tunnelling between two magnetic materials, the quantity to be determined is the junction conductance for parallel versus antiparallel orientation of the electrode magnetizations. The relative change of the conductance gives a measure for the product of the spin polarizations of the electrode materials. This technique has been treated in a number of theoretical papers [3]. Experiments have been performed with planar junctions [4] as well as with an STM in an ultra-high-vacuum environment [5].

(iii) Due to the spin–orbit interaction, by optical means a spin selectivity can be achieved in a nonmagnetic semiconductor. For that reason also a III–V semiconductor material can be used in a spin-polarized tunnelling experiment. For example, the injection of nonequilibrium spin-polarized carriers can be detected due to the emission of polarized radiation. In an STM the emission of polarized luminescence due to spin-polarized tunnelling has already been observed with ferromagnetic tips and a GaAs sample [6]. On the other hand, spin-polarized carriers can be created by photoexcitation with circularly polarized light—so-called optical spin orientation [7]. The possibility of using optical spin orientation in GaAs for the purpose of spin-polarized tunnelling has been discussed in several publications [8, 13]. These ideas originate from the successful operation of spin-polarized electron sources based on optical excitation of caesium-covered p-type GaAs (see, e.g., [14]). Pioneering experiments with planar solid-state junctions were performed in our group [15]. The application of photoexcited GaAs for magnetic imaging has become a hot issue with the development of cleaved GaAs tips for STM operation, under ultra-high-vacuum conditions [16] as well as under ambient conditions [17, 18].

In this paper we will be concerned with the usage of optical spin orientation in GaAs in order to achieve spin selectivity in a tunnelling arrangement. First, a model description of spin-dependent transport will be given. This model includes the subsurface transport processes in the semiconductor and spin relaxation at the semiconductor surface. Experimental results obtained with planar junctions will be presented and analysed. Finally we discuss the application of optical spin orientation in GaAs for magnetic imaging in an STM.

2. The model for spin-dependent transport

In this section we describe a model for spin-dependent transport in a tunnel junction between a metallic and a semiconductor material, when optical spin orientation is applied. This system is rather complicated, because one should not only consider the tunnel current between the metal and the semiconductor surface, but also the electron and hole currents in the semiconductor subsurface region. The tunnelling current has already been treated theoretically by Molotkov [11] in a Green's function formalism, and by Laiho and Reittu [12] for plane electronic waves; we will describe the tunnelling current by the transfer Hamiltonian approach [19], in a convenient form for a modulation experiment. To

our knowledge, the spin-dependent transport in the semiconductor, including the subsurface electron and hole currents, the surface states and spin relaxation therein, has not been treated elsewhere.

In a III–V semiconductor like GaAs, optical spin orientation involves photoexcitation with light of circular polarization [7]. At the direct gap of GaAs the conduction band is predominantly formed of Ga-derived wavefunctions with s symmetry, whereas the valence band consists of As-derived wavefunctions of p symmetry. Because of the spin–orbit interaction in the valence band, the optical transition probabilities are such that circularly polarized photons with an energy close to the bandgap give a maximum spin polarization of 50% in unstrained GaAs [20]. An important consequence of optical spin orientation is that in the semiconductor the energy distribution of charge carriers deviates from equilibrium and is unequal for the two spin orientations, the latter quality being essential for a spin-polarized tunnelling experiment.

In the following, we will first consider the spin-dependent tunnelling current flowing between a magnetic material and a semiconductor surface, for a given spin-dependent energy distribution of carriers at the semiconductor surface. Next, we will present a model description of the mechanisms that determine the size of the spin dependence of the energy distribution function at the semiconductor surface, the so-called semiconductor surface spin-splitting.

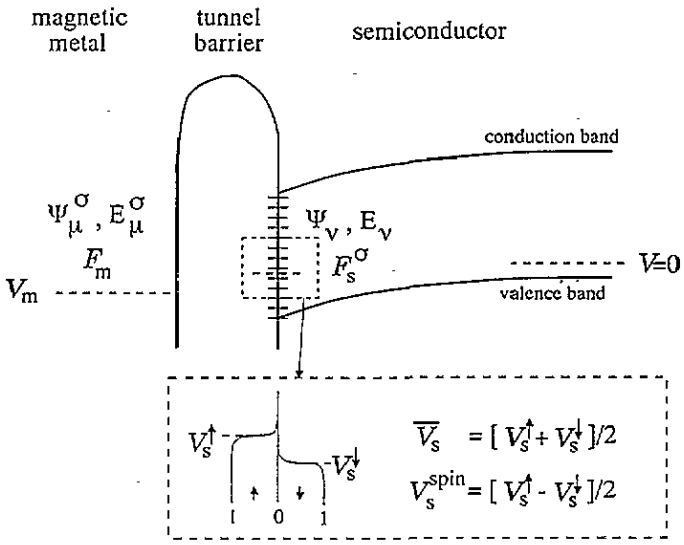

Figure 1. A one-dimensional electronic energy diagram of a tunnel junction between a magnetic metal and a p-type semiconductor. The 'blow-up' shows the occupation of the surface states for the two spin directions. The spin-dependent quasi-Fermi level is represented by V_s^σ. See the text for further explanations. The picture is not to scale, because in general the band-bending region in the semiconductor is considerably larger than the tunnel barrier width.

2.1. Spin-polarized tunnelling

The present derivation of the spin-dependent tunnelling current is based on the transfer Hamiltonian approach, a first-order perturbation method that applies in the case of a low tunnel barrier transparency [19]. As depicted in figure 1, the magnetic electrode is described by single-particle spin-dependent wavefunctions ψ_μ^σ with energies E_μ^σ. The superscript σ

indicates the spin orientation with respect to a given quantization axis (parallel or spin up equals ↑, antiparallel or spin down equals ↓); we will use identical spin-quantization axes for the two materials. It is assumed that the tunnel current and optical excitation represent a negligible perturbation to the metallic electrode; for that reason the energy distribution function in the magnetic metal ($\mathcal{F}_m$) does not depend on the electron spin [21]. Since the semiconductor is not magnetic, the semiconductor surface is described by the spin-independent wavefunctions ψ_ν with energies E_ν; however, due to optical spin orientation the carriers at the semiconductor surface follow a spin-dependent energy distribution ($\mathcal{F}_s^\sigma$).

In a good tunnel barrier no scattering centres are available such that the electron energy and the electron spin are conserved during the tunnelling process. In that case, the tunnel current (I_t^σ) for spin orientation σ from the magnetic material to the semiconductor surface can be expressed as follows:

$$I_t^\sigma = \frac{1}{-e}\int d\varepsilon\ \left[\mathcal{F}_m(\varepsilon + eV_m) - \mathcal{F}_s^\sigma(\varepsilon)\right] G_t^\sigma(\varepsilon) \tag{1}$$

$$G_t^\sigma(\varepsilon) = \frac{2\pi e^2}{\hbar}\sum_{\mu\nu}\delta(\varepsilon + eV_m - E_\mu^\sigma)\,\delta(\varepsilon - E_\nu)\,|M_{\mu\nu}^\sigma|^2 \tag{2}$$

$$M_{\mu\nu}^\sigma = \frac{\hbar^2}{2m}\int dS\cdot\left[\psi_\mu^{\sigma *}\nabla\psi_\nu - \psi_\nu\nabla\psi_\mu^{\sigma *}\right] \tag{3}$$

where e is the absolute magnitude of the electron charge. The magnetic electrode is at the externally applied potential V_m. The energy zero is given by the Fermi level in the semiconductor bulk. The function $G_t^\sigma(\varepsilon)$ takes account of all energy-conserving tunnelling transitions at energy ε, for states with spin orientation σ. As we will see, G_t^σ closely relates to the differential tunnelling conductance. $M_{\mu\nu}^\sigma$ is the well known tunnelling matrix element; the surface integral ($\int dS$) is evaluated inside the barrier separating the two materials. The matrix element takes account of the overlap of the wavefunctions of the respective electrode materials. This parameter is spin dependent because the wavefunctions of the magnetic material depend on the electron spin. Calculation of the total tunnel current yields

$$I_t = \sum_\sigma I_t^\sigma = \frac{1}{-e}\int d\varepsilon\ \underbrace{\{[G_t^\uparrow + G_t^\downarrow][\mathcal{F}_m - \overline{\mathcal{F}}_s]}_{\text{spin integrated}} - \underbrace{[G_t^\uparrow - G_t^\downarrow][\mathcal{F}_s^\uparrow - \mathcal{F}_s^\downarrow]/2\}}_{\text{spin selective}} \tag{4}$$

where $\overline{\mathcal{F}}_s \equiv [\mathcal{F}_s^\uparrow + \mathcal{F}_s^\downarrow]/2$ is the spin-averaged distribution function at the semiconductor surface. The first term takes account of the spin-integrated tunnel current. The second term is present in the case of a spin-polarized magnetic material ($G_t^\uparrow \neq G_t^\downarrow$) *and* a spin imbalance in the semiconductor ($\mathcal{F}_s^\uparrow \neq \mathcal{F}_s^\downarrow$). An expression similar to equation (4) was derived in [11]. In the following we will assume that at the semiconductor surface each spin subsystem is close to thermal equilibrium, because the processes of carrier capture and energy relaxation are generally very efficient at surfaces with surface states [22]. This means that the spin subsystems approximately follow an energy-shifted Fermi–Dirac distribution: $\mathcal{F}_s^\sigma(\varepsilon) \simeq f(\varepsilon + eV_s^\sigma)$, where V_s^σ is the spin-dependent surface potential. As indicated in figure 1, this allows for the definition of the spin-averaged surface potential: $\overline{V}_s \equiv [V_s^\uparrow + V_s^\downarrow]/2$, and of the surface spin-splitting: $V_s^{spin} \equiv [V_s^\uparrow - V_s^\downarrow]/2$.

In our experiments a modulation of optical polarization and/or of optical intensity is applied. As a result, the spin-dependent distribution function at the semiconductor surface becomes time dependent with the following form: $\mathcal{F}_s^\sigma(t) = \mathrm{Re}\{\mathcal{F}_s^\sigma + \Delta\mathcal{F}_s^\sigma \exp(i\omega t)\}$, where ω is the modulation frequency. The associated time-dependent surface potential

becomes: $V_s^\sigma(t) = \mathrm{Re}\{V_s^\sigma + \Delta V_s^\sigma \exp(i\omega t)\}$. To first order in the modulation amplitudes, with equation (4) we find the following modulation of the total tunnelling current:

$$\Delta I_t \propto -\{\underbrace{[G_t^\uparrow + G_t^\downarrow]\ \Delta\overline{V_s}}_{\text{spin integrated}} + \underbrace{[G_t^\uparrow - G_t^\downarrow]\Delta V_s^{\text{spin}}}_{\text{spin selective}}\} \tag{5}$$

where $\Delta\overline{V_s} = [\Delta V_s^\uparrow + \Delta V_s^\downarrow]/2$, and $\Delta V_s^{spin} = [\Delta V_s^\uparrow - \Delta V_s^\downarrow]/2$. The spin-selective contribution of equation (5) can also be written as follows:

$$\Delta I_t = -G_t \mathcal{P}(G_t)\ \Delta V_s^{\text{spin}} \tag{6}$$

where $G_t \equiv G_t^\uparrow + G_t^\downarrow$ and $\mathcal{P}(G_t) \equiv [G_t^\uparrow - G_t^\downarrow]/G_t$. The negative sign in equation (6) results from the definition of the direction of current flow. $\mathcal{P}(G_t)$ is the normalized polarization of the spin-dependent tunnel conductance. This quantity was evaluated by Laiho and Reittu [12, 13] for a two-band free-electron ferromagnet in a planar junction, showing that the size of $\mathcal{P}(G_t)$ depends not only on the bulk bandstructure, but also on the tunnel barrier height and shape. Experiments [1] as well as calculations [12] indicate that $\mathcal{P}(G_t)$ can be tens of per cent for materials like Fe, Co, and Ni.

An ideal optical spin-orientation experiment involves only a modulation of the surface spin-splitting (ΔV_s^{spin}), not a modulation of the spin-averaged surface potential ($\Delta\overline{V_s} = 0$). However, in the case of an unwanted modulation of the optical power, the spin-averaged potential will also modulate [23]. This can for example be due to the magneto-optical Kerr/Faraday effect [31]. In our experiments, we find that ΔV_s^{spin} and $\Delta\overline{V_s}$ are of comparable size, namely of the order of a few per cent of $\overline{V_s}$. In order to separate the spin-selective from the spin-integrated contributions to the current modulation, an additional technique is required. In principle the separation can be achieved by varying the photon energy, the tunnel barrier width, and the applied voltage. In addition to the above-described modulation of tunnel current, displacement currents can appear (see [24]). These signals are not of interest here, since they carry no spin selectivity.

2.2. *Semiconductor surface spin-splitting*

The spin dependence of the energy distribution function at the semiconductor surface (the so-called surface spin-splitting) is determined by the flow of spin-polarized minority and majority carriers in the semiconductor subsurface region [25], the spin-relaxation rate at the semiconductor surface, and the spin-polarized tunnel current from the semiconductor surface to the magnetic electrode. In order to calculate the semiconductor spin-splitting, we present a one-dimensional spin-dependent transport model. This model is based on the work of [24], where the electron spin was still ignored. As was already pointed out in figure 1, the metal–semiconductor junction is modelled as a device with three 'electrodes': the metallic electrode, the semiconductor surface states, and the semiconductor bulk. The metal is biased with respect to the semiconductor bulk Fermi level by the externally applied voltage V_m. Between the metal and the surface states a tunnel barrier is present; the surface states and semiconductor bulk are separated by a Schottky barrier, i.e. the semiconductor subsurface band-bending region. The band-bending region represents a barrier for majority-carrier transport; at the same time, it constitutes an accelerating field for photoexcited minority carriers.

The important spin-polarized currents are given by: the current density of photoexcited carriers (J_p^σ), the majority-carrier current density through the Schottky barrier (J_s^σ), and the tunnel current density (J_t^σ). We define J_t^σ to flow from the magnetic electrode to the

semiconductor surface; J_p^σ and J_s^σ represent flow from the semiconductor surface to the semiconductor bulk. Let the density of spin-up (spin-down) electrons at the semiconductor surface be given by $N_{ss}^{\uparrow}$ ($N_{ss}^{\downarrow}$). The excess density of spin-up electrons is defined as $N_{ss}^{spin} \equiv N_{ss}^{\uparrow} - N_{ss}^{\downarrow} = -eV_s^{spin}D_{ss}$, where D_{ss} is the total density of surface states (units $m^{-2}\ J^{-1}$). The density of surface states is assumed to be uniform over the range of interest (as for example applies to the native oxide on GaAs [26]). When at the surface the spin lifetime is given by τ^{spin}, the density of current flowing from the spin-up to the spin-down spin subsystem at the surface becomes

$$J_{ss}^{spin} = \frac{-eN_{ss}^{spin}}{\tau^{spin}} = \frac{e^2 D_{ss}}{\tau^{spin}} V_s^{spin} \equiv \tilde{G}_{ss}^{spin} V_s^{spin} \tag{7}$$

where $\tilde{G}_{ss}^{spin} \equiv e^2 D_{ss}/\tau^{spin}$ is the spin conductance between the spin subsystems at the semiconductor surface. The tilde denotes that the conductance is defined per unit area. Bookkeeping of the flow of spin and charge yields the following equations for the spin-dependent current densities at the semiconductor surface:

$$J_p^{\uparrow} + J_s^{\uparrow} - J_t^{\uparrow} + J_{ss}^{spin} = 0 \qquad J_p^{\downarrow} + J_s^{\downarrow} - J_t^{\downarrow} - J_{ss}^{spin} = 0. \tag{8}$$

Adding and subtracting these equations, and using the normalized spin polarizations of the respective currents, we find

$$J_p + J_s - J_t = 0 \qquad J_p\mathcal{P}(J_p) + J_s\mathcal{P}(J_s) - J_t\mathcal{P}(J_t) + 2\tilde{G}_{ss}^{spin}V_s^{spin} = 0 \tag{9}$$

where $J_i \equiv J_i^{\uparrow} + J_i^{\downarrow}$ and $\mathcal{P}(J_i) \equiv [J_i^{\uparrow} - J_i^{\downarrow}]/J_i$, $i \in \{p, s, t\}$. The so-called photoamperic mode of operation of the metal–semiconductor tunnel junction (see [24]) refers to the situation in which the tunnel barrier represents a far higher conductance than the Schottky barrier, i.e. $J_t \simeq J_p$, and $|J_s| \ll |J_p|$. In that limit the size of the tunnelling current (J_t) is given by the size of the photocurrent (J_p), and is not affected by the polarization of the photocurrent $\mathcal{P}(J_p)$. Or to put it differently, whatever the polarization of the photocurrent, all the photoexcited carriers will be transported into the metallic electrode, because the Schottky barrier is too high. This is an undesirable situation for a spin-polarized tunnelling experiment, where spin sensitivity is wanted in the total tunnelling current. In order to maximize the spin sensitivity in the total tunnelling current, we should operate in the so-called photovoltaic regime (see [24]), where the tunnel barrier conductance is lower than the conductance of the Schottky barrier. Then the tunnel current (J_t) is negligible with respect to the photocurrent, and $J_s \simeq -J_p$. This situation has the important advantage that the spin-splitting at the semiconductor surface is only determined by the photocurrent and the Schottky majority-carrier current, independently of the tunnelling current properties.

Let us calculate the size of the spin-splitting at the semiconductor surface for *p-type* GaAs in the *photovoltaic* mode of operation. By optical spin orientation in GaAs, the spins of the electrons as well as the hole spins are oriented in principle. However, due to the spin–orbit interaction a strong coupling exists between the hole's angular momentum and its quasimomentum (k), resulting in a loss of the hole spin orientation on the time-scale of the momentum relaxation time ($\tau_p \sim 10^{-13}$ s); in the conduction band this strong coupling is absent, causing the electron spin lifetime to be many orders of magnitude larger [27]. In p-type GaAs the bands are generally bending downward from the bulk toward the surface, which drives the optically oriented electrons toward the surface [28]. In the photovoltaic mode of operation, this flow of electrons (the minority-carrier current J_p) is balanced by the hole current that flows through the Schottky barrier (the majority-carrier current J_s); the latter is given by thermally assisted transport over the electrostatic barrier and subsequent surface recombination [29, 30]. Since the holes are hardly polarized, we can neglect the

spin dependence of the hole energy distribution in the semiconductor bulk; in addition, for a small spin-splitting the surface recombination velocity does not depend on the electron spin. In other words, in p-type GaAs we can to first order neglect the polarization of the majority-carrier current $\mathcal{P}(J_s)$ with respect to the polarization of the minority-carrier current $\mathcal{P}(J_p)$. In that case, using (7) and (9) in the photovoltaic mode of operation ($J_t = 0$), we find the following expression for the spin-splitting of the surface potential:

$$V_s^{spin} = -\mathcal{P}(J_p)J_p\frac{\tau^{spin}}{2e^2D_{ss}}. \tag{10}$$

Thus, for a maximum spin-selective tunnelling current (cf. equation (6)), it is appropriate to use p-type GaAs in the photovoltaic mode of operation, with a large magnitude and polarization of the photocarrier current, a large surface spin lifetime, and a low density of surface states.

In summary, we have analysed the spin-dependent tunnelling current in a tunnel junction between a magnetic material and a semiconductor, where in the latter a modulation of spin orientation was established by optical means. In the semiconductor, account was taken of the polarized hole and electron currents, and the carrier capture and transport in the surface states. For future directions, it will be of interest to model the polarization of the majority-carrier current, which will be important for large values of the surface spin-splitting and for n-type materials [28].

3. Experiments

This section deals with experiments on planar ferromagnet/insulator/semiconductor junctions. The sample substrate is GaAs, with a tunnel barrier of Al oxide or AlAs. The ferromagnet is a Co thin film, with or without an ultrathin τ-MnAl film inserted. In these junctions the light traverses the magnetic thin film before reaching the semiconductor material. This implies that the magneto-optical Faraday effect [31] can be of importance. Upon transmission through the magnetic film, the change of optical *polarization* is of the order of 10^{-2}, which can safely be neglected. More importantly, the Faraday effect results in a helicity dependence of the transmission of optical *power* into the semiconductor material, an effect that is also of the order of 10^{-2}. In other words—when applying a technique of modulation of optical polarization—concurrently with a modulation of the spin orientation of the electrons, the amount of photoexcited carriers also is modulated. In the context of equation (5), this was referred to in terms of the spin-selective and spin-integrated contributions to the current modulation. The two contributions can be separated by varying the photon energy and by comparing devices with different tunnel barrier thicknesses [32], as will be described in the following.

3.1. GaAs(Al/Al$_2$O$_3$)Co

The samples with an Al_2O_3 tunnel barrier were prepared in an electron beam evaporation system. The substrates were GaAs(110) surfaces cleaved under ambient conditions. The exposure of the GaAs to the ambient gives an oxidic layer with a thickness of about a nanometre and a high density of surface states [26]. The GaAs was p-type (Zn doped) or n-type (Si doped) with doping densities in the range 10^{17} to 10^{18} cm^{-3}. First, on the substrate an Al film was deposited; in order to prevent island growth the substrates were cooled with liquid nitrogen. Subsequently, for a couple of hours the Al was oxidized by a glow discharge in oxygen at a pressure of ~0.1 Torr, while the sample was allowed to

reach room temperature. Similar procedures are known to produce good tunnel barriers with a thickness of about 2 nm (see, e.g., [1, 4]). Finally, 15 nm of Co and a 5 nm Au cap layer were deposited. A quartz microbalance was used to measure the film thickness. All depositions were carried out at approximately 0.2 nm s^{-1} with a chamber pressure in the 10^{-7} Torr region.

3.2. GaAs(AlAs)τ-MnAlCo

The samples with an AlAs tunnel barrier were prepared by molecular beam epitaxy (MBE) on GaAs(001) substrates. The growth was done in two separate MBE chambers, the first containing nonmagnetic elements only, the second including some magnetic elements. The base pressure of the chambers was in the high 10^{-11} and low 10^{-10} Torr region, respectively. The growth rates were controlled by setting the atomic or molecular fluxes to the desired value, and by measuring the RHEED (reflection high-energy electron diffraction [33]) intensity oscillations *in situ*. The RHEED pattern served to monitor the surface structure and verify the epitaxial growth of the layers. In the first chamber a p-doped buffer layer (C doped, 10^{18} cm^{-3}) 1 μm thick was deposited on a p-type GaAs(001) substrate, at a growth temperature of 560 °C and a growth rate of ~1 μm per hour. The substrate was then cooled to room temperature and an As passivation layer was deposited for two hours to protect the sample from the atmosphere during transfer to the second chamber. To regain the p-doped GaAs surface, in the second chamber the substrate was heated to evaporate the As protection layer and some remaining oxygen. An epitaxial AlAs tunnel barrier was then deposited (20 nm AlAs for sample M171, and 2 nm AlAs for sample M172) at a substrate temperature of 580 °C.

There is a limited set of ferromagnetic materials that can be grown epitaxially on AlAs, one of these materials being τ-MnAl. The latter is a metastable phase of the intermetallic MnAl system, with a composition ratio Mn/Al of about 55/45 [34]. τ-MnAl has a tetragonal unit cell, and is well lattice matched to GaAs. On the AlAs tunnel barrier an ultra-thin τ-MnAl layer was deposited (as a so-called template) for Co epitaxy. The template involved the deposition of 5 alternating monolayers of Mn and Al (2.5 so-called bilayers) to form an amorphous layer, and annealing at ~250 °C to form a crystalline template [35]. This template allows for growth of the forced bcc phase of Co [36–38]. 4 nm of Co were deposited at a substrate temperature of ~250 °C and a rate of 75 nm h^{-1}. The growth was concluded with an amorphous GaAs passivation layer (15 nm) deposited at ~80 °C.

3.3. Experimental arrangement

As sketched in figure 2, in our experiments the propagation direction of the incident optical beam was collinear with the applied magnetic field, and (within about 5°) also collinear with the sample normal. For the above-mentioned ferromagnetic thin films the easy magnetization orientation is in the film plane. A magnetization component parallel to the incident beam was created by an external magnetic field of 300±30 kA m^{-1}, supplied by an electromagnet with a hole bored through one pole for optical access. Sample sizes were a few mm^2. Low-impedance back contacts to the substrate were made by InGa droplets. Typical excitation levels were a few mW focused to a spot diameter of about 50 μm, yielding closed-circuit currents (I) in the μA range. Different photon energies were provided by an Ar-ion (for photon energies of 2.71, 2.54 or 2.41 eV), a HeNe (1.96 eV), and an AlGaAs (1.52 eV) laser. The helicity dependence of the current was determined by modulating the light between positive and negative helicity, and measuring the response with a lock-in amplifier

(ΔI). A reversal of the magnetic field was employed in order to subtract minor signals of nonmagnetic origin (electrical pickup or a residual intensity modulation due to imperfect optical alignment).

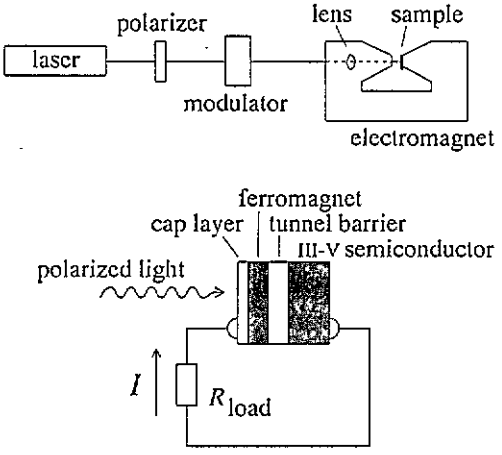

Figure 2. The experimental arrangement (top) and device construction (bottom).

For all devices we measured the current response (R) to a modulation of incident optical power (ΔP), where the response is defined as $R = [\Delta I/I]/[\Delta P/P]$. For junctions with a tunnel barrier, we observed that the response became larger than unity and phase shifted at modulation frequencies higher than about one kilohertz; this we attribute to the appearance of a displacement current that flows through the tunnel barrier. Since in the following experiments we want to detect direct currents only, we chose the modulation frequency low enough to ensure that the response (R) was unity. The application of an external bias of more than a few tenths of a volt across the samples often gave rise to a sudden lowering of the device resistance. This is indicative of the formation of low-resistance spots, most probably at the sample edges. We verified that the helicity asymmetry $\Delta I/I$ was not sensitive to a sudden change of the device resistance; this can be understood from the fact that a low-resistance spot simply operates as a resistor in parallel to the externally attached load resistance (R_{load} in figure 2). In the following measurements the load resistance was lower than the internal resistance of the junctions, and no external bias was applied to the junctions.

4. Results and discussion

4.1. GaAs(Al/Al_2O_3)Co

The top panel of figure 3 shows the helicity asymmetry $\Delta I/I$ as a function of photon energy, for samples of different growth batches. Devices A are constructed without an Al/Al_2O_3 interlayer. As was pointed out with equation (9), in devices without a tunnel barrier the spin-dependent effects should be minimized, such that only magneto-optical effects can give a helicity asymmetry to the tunnel current. For these devices, the dashed line (A′) represents a calculation of the helicity asymmetry of the optical power absorbed in the semiconducting substrate; the optical propagation and absorption in the layered system was calculated with a matrix formalism [39] that takes account of the (polarization-dependent) complex refractive indices of the layers [40]. The optical constants were taken from the literature [41, 42]. As can be seen from comparison of curves A to the calculation (A′), this description of

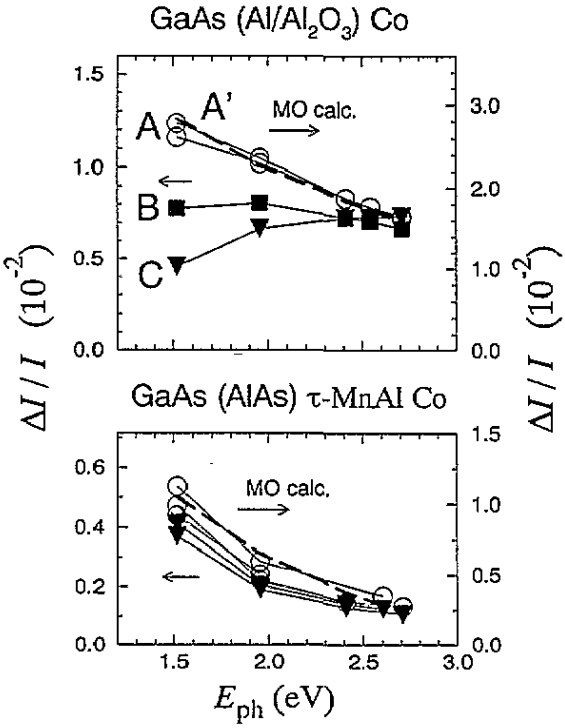

Figure 3. Helicity asymmetry $\Delta I/I$ as a function of photon energy E_{ph}. *Top:* Al_2O_3 devices. Curves A represent the measured asymmetries for devices with no Al/Al_2O_3 interlayer. Curve B refers to a device of incompletely oxidized Al (~6 nm Al and ~2 nm Al_2O_3). Curve C gives the results for a completely oxidized Al interlayer (~4 nm Al_2O_3). The dashed line A' represents a magneto-optical calculation of the helicity asymmetry of optical power absorbed in the GaAs substrate in the absence of an Al/Al_2O_3 interlayer (MO calculation, right-hand scale). *Bottom:* AlAs devices. The circular symbols represent data for samples with a 2 nm AlAs barrier, whereas the triangular symbols refer to samples with a 20 nm AlAs barrier. The dashed line represents a magneto-optical calculation of the helicity asymmetry of optical power absorbed in the GaAs substrate (MO calculation, right-hand scale). Solid lines are guides to the eye.

the magneto-optical signal is quite accurate; the difference between the magnitude of the measured values (left-hand scale) and the calculated values (right-hand scale) is due to the incomplete magnetization of the ferromagnetic thin film, as we confirmed by measurements at higher fields.

Device B was prepared by depositing a single 8 nm Al film, that was subsequently oxidized. The Al_2O_3 layer has a thickness of ~2 nm [1, 4], so ~6 nm of Al remains between the GaAs and the Al_2O_3. Due to the conducting Al film on the semiconductor surface, devices prepared in this way are not expected to show maximum spin-dependent transmission effects (this was not yet recognized in our previous publication in [15]). This expectation is based on the high density of states at the semiconductor surface, which according to equation (10) gives a low spin-splitting at the semiconductor surface. Additional magneto-optical calculations on the structure of device B show that—when compared to that for device A—the helicity asymmetry is reduced by 20% at 1.5 eV and is modified by less than 4% at 2.7 eV. Since these reductions are approximately observed, we conclude that device B also shows a helicity asymmetry mainly due to magneto-optical effects.

Device C is composed of a double barrier, i.e. twice an Al film of ~2 nm was deposited and oxidized. Since these Al films were so thin, we can assume that they were completely oxidized [1, 4]. Additional magneto-optical calculations on the structure of device C show that—compared to that of device A—the magneto-optical contribution to the helicity asymmetry is changed by less than 4% in the photon energy range of interest. In other words, the strong deviations of curve C from curve A—at 1.5 eV photon energy a reduction of helicity asymmetry of 60%—cannot be explained by magneto-optical effects. The striking feature is that the deviations are largest at near-bandgap excitation (i.e. toward 1.42 eV), and that curve C converges with curve A at higher photon energy: qualitatively the same wavelength dependence is observed for spin-polarized photoemission from caesium-covered GaAs [7, 43, 44]. This wavelength dependence is mainly determined by the spectral behaviour of the optical dipole transitions and spin-relaxation mechanisms [7]. Following our model description (cf. equation (5)) we attribute the observed deviations of curve C from curve A to a spin-selective current contribution, i.e. the occurrence of spin-dependent tunnelling of optically oriented carriers.

At 1.5 eV photon energy, the measured difference in helicity asymmetry ($\Delta I_t/I_t$) between curves C and A of figure 3, upper panel, amounts to $(7 \pm 1) \times 10^{-3}$. Let us analyse this observation with our model of spin-dependent transport, in order to deduce the spin-splitting at the semiconductor surface. It follows from other measurements on Al_2O_3 tunnel barriers [45] that the differential tunnelling conductance is rather constant in the case of a voltage drop of less than a tenth of a volt, and that for higher voltages the differential conductance increases with a quadratic dependence on the voltage drop. In other words, a lower limit to the differential tunnelling conductance [46] is given by $G_t \geqslant I_t/[V_m - \overline{V}_s]$; because no external voltage was applied in these experiments ($V_m = 0$), with equation (6) we find that the relative spin-splitting at the semiconductor surface is either given by

$$\frac{\Delta V_s^{spin}}{\overline{V}_s} = \frac{1}{\mathcal{P}(G_t)} \frac{\Delta I_t}{I_t} \tag{11}$$

or is of a lower absolute magnitude. In earlier spin-polarized tunnelling measurements with fully magnetized Co, a spin polarization of $|\mathcal{P}(G_t)| = 0.35$ was detected [1]; in our experiment, along the direction of the incident beam the magnetization was found by measurement to be less than 50% of its saturation value, so a reasonable estimate for $|\mathcal{P}(G_t)|$ is 0.15 ± 0.05. Using the measured value for $\Delta I_t/I_t$, with equation (11) we deduce that the relative spin-splitting at the semiconductor surface ($\Delta V_s^{spin}/\overline{V}_s$) was lower than or equal to $(5 \pm 2) \times 10^{-2}$ in this experiment. As was pointed out with equations (9) and (10), the value of the surface spin-splitting (V_s^{spin}) is not only determined by the photoexcited minority-carrier current, but also by the surface spin relaxation, the Schottky majority-carrier current, and the tunnelling current. The magnitude of the spin-averaged potential ($\overline{V}_s$) strongly depends on the Schottky barrier height (cf. [24]). In our devices the determination of the spin-averaged potential ($\overline{V}_s$) was inhibited due to the presence of low-resistance spots, so we are unable at present to further analyse the previous experimental result in the perspective of our model description.

Finally, we tentatively analyse the sign of the spin polarization of the tunnel conductance that follows from our measurement. In magnetic materials, it is common usage to define the electron spin orientation to be positive if the electron belongs to the majority-spin type, i.e. if the magnetic moment of the electron is aligned with the sample magnetization (see, e.g., [1, 47]). For electrons the orientation of the spin magnetic moment is opposite to the spin orientation. Thus, to be consistent with the above convention, we should choose the spin-quantization axis of the electronic wavefunctions *opposite* to the direction of the

external magnetic field. In the following analysis we will define the spin-quantization axis of the electronic wavefunctions to be equal to the sample normal, and choose the external magnetic field to be parallel to the propagation direction of the incident beam. In that case, it follows from other measurements [48] that the magnetic circular dichroism of Co is such that light of negative helicity is less strongly absorbed than light of positive helicity. This implies that due to magneto-optical effects, in our junctions a higher photocurrent is measured for light of negative helicity. When light of near-bandgap photon energy and negative helicity is used, the electron spins are preferentially oriented parallel to the quantization axis [7]: $V_s^{spin}/\overline{V}_s > 0$ if $V_m = 0$. Since we attributed a *decrease* of $\Delta I/I$ to spin-polarized tunnelling, using equation (11) we derive that the spin polarization of the tunnel conductance $\mathcal{P}(G_t)$ was of negative sign. In earlier spin-polarized tunnelling measurements with superconducting Al and an Al_2O_3 tunnel barrier, with fully magnetized Co a spin polarization of +0.35 was detected, corresponding to predominantly tunnelling of majority-spin electrons at the Co Fermi level [1]. It is well known that different measurement techniques can give a different sign for the spin polarization; for example, spin-polarized photoemission from Co shows predominantly minority-spin electrons at the Fermi level [49, 50]. Comparing our measurement with the measurements of [1], it may well be that in the respective experiments the electron tunnelling occurs at a different energy.

4.2. GaAs(AlAs)τ-MnAlCo

The bottom panel of figure 3 shows the helicity asymmetry $\Delta I/I$ as a function of photon energy for devices with an AlAs tunnel barrier, a τ-MnAl template, and a Co thin film. The circular symbols represent measurements on samples with a 2 nm AlAs barrier, whereas the triangular symbols were measured on samples with 20 nm of AlAs. As for the calculations for the Al_2O_3 junctions, the dashed line represents a magneto-optical calculation of the helicity asymmetry of the optical power absorbed in the semiconducting substrate; we verified that the calculated helicity asymmetry is hardly affected by the thickness of the AlAs interlayer.

In the case of a spin-polarized tunnelling effect, we expect to observe a different helicity asymmetry of the current for samples with a thin and with a thick tunnel barrier, as was discussed using equation (9); this is not observed in figure 3. Futhermore, we observe that the measured data are close to the calculated magneto-optical curve. In other words, the data can be explained by magneto-optical effects only, and we find no evidence for spin-polarized tunnelling within the measurement uncertainty of $\sim 10^{-3}$.

In view of the previous results, bandstructure calculations of τ-MnAl were performed (for details, refer to [51]). For both spin directions, figure 4 shows the calculated energy bands and figure 5 the calculated density of states. The spin polarization of the total number of electrons at the Fermi level is $\mathcal{P}_N \equiv [N^{\uparrow} - N^{\downarrow}]/[N^{\uparrow} + N^{\downarrow}] = -0.37$, where $N^{\uparrow(\downarrow)}$ is the number of majority- (minority-) spin electrons at the Fermi level. This polarization mainly results from the strongly spin-split Mn 3d bands in the ΓXM plane of the Brillouin zone, representing wavefunctions that are itinerant in the planes containing the Mn atoms.

4.3. Bandstructure calculations

Concerning the implications of the calculated bandstructure for a tunnelling experiment, it is important to realize that tunnelling is a direction-specific probing technique. In our junctions, the tunnelling direction is given by a cone of less than five degrees around the sample normal [56], which is the c-axis of the τ-MnAl unit cell. Thus, the most important

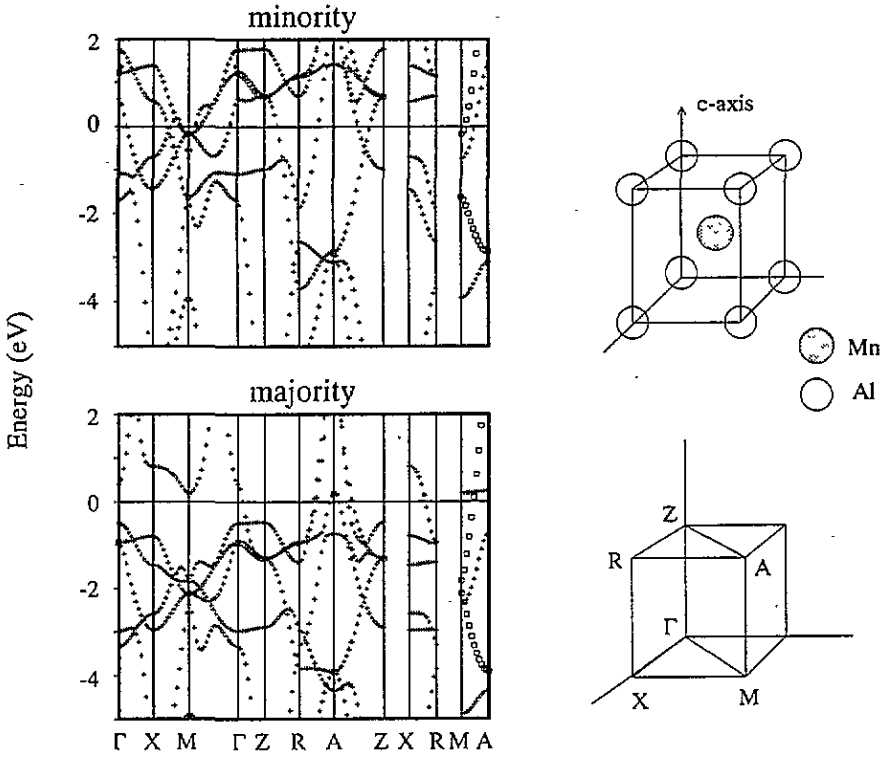

Figure 4. Electron energy bands of bulk τ-MnAl along high-symmetry directions, calculated with the localized spherical wave (LSW) method. Crosses represent nondegenerate states, whereas squares represent doubly degenerate states. On the right-hand side are indicated the τ-MnAl unit cell and the irreducible part of the Brillouin zone.

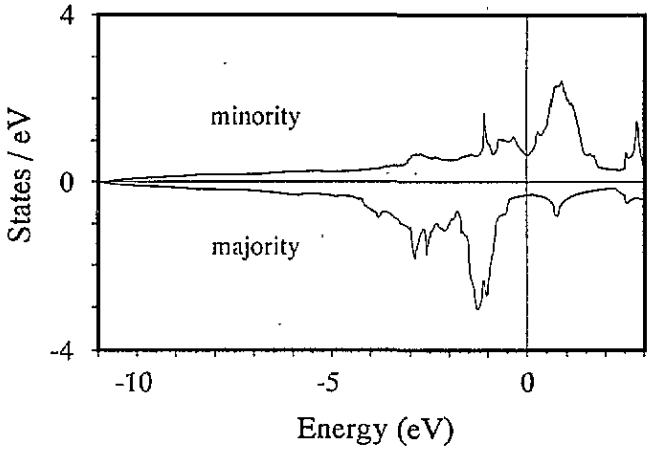

Figure 5. The calculated density of states per unit cell in bulk τ-MnAl, for the minority and majority spins. Zero energy corresponds to the Fermi level.

contributions to the spin-dependent tunnelling conductance G_t^σ (defined in equation (2)) are given by the energy bands that are dispersive in the z-direction of the Brillouin zone, i.e. the bands that cross the high-symmetry directions ΓZ, MA and XR. Along these directions

we observe a rather similar bandstructure for the majority- and minority-spin electrons: at the Fermi level the crossings of respectively three and four states are involved; when constructing the Fermi surface, it appears that for both spin directions the above-mentioned axes are crossed by three Fermi sheets of comparable character. This is in strong contrast to the bandstructure polarization in the ΓXM plane. In other words, along the xy-planes the conductance is strongly spin polarized, whereas perpendicular to these planes a spin polarization is hardly present. We also performed bandstructure calculations (not shown) for the structure of our samples (an ultra-thin τ-MnAl layer sandwiched between GaAs and Co). These calculations indicated that the electronic structure of the Mn and Al atoms adjacent to the GaAs is similar to the bulk τ-MnAl electronic structure, and so the previous analysis also applies to the junctions of our experiments.

5. Summary and conclusions

In this paper we presented a model for spin-polarized transport in a photoexcited tunnel junction between a magnetic metal and a semiconductor, where the semiconductor charge carriers are polarized by optical orientation. The semiconductor surface was described in terms of a spin-dependent distribution function or quasi-Fermi level V_s^σ. The model clearly demonstrates that the spin-selective contribution to the total tunnelling current is proportional to the product of the spin dependence of the tunnelling conductance $(G_t^\uparrow - G_t^\downarrow)$ and the spin-split quasi-Fermi level at the semiconductor surface $(V_s^\uparrow - V_s^\downarrow)$. The sensitivity of the total tunnelling current is maximized if the tunnel barrier conductance is lower than the Schottky barrier conductance, i.e. when the tunnel current represents a negligible disturbance to the semiconductor. In that case, in a p-type material the spin-splitting at the semiconductor surface is proportional to the density and the polarization of the photoexcited electrons, and to the surface spin lifetime, and inversely proportional to the density of surface states.

Experimental results were shown for planar tunnel junctions made of GaAs. A technique of polarization modulation was employed, and the resulting tunnel current modulation was detected. A complication is that the current modulation is caused by optical spin orientation and spin-dependent transmission over the tunnel barrier, *as well as* by a modulation of optical power absorbed in the semiconductor. The power modulation is due to the magneto-optical Kerr/Faraday effect. In our samples the magneto-optical contribution to the helicity asymmetry of the photocurrent (the Faraday effect) is of the order of 10^{-2}, which is larger than the contribution attributed to spin-polarized transmission. Nevertheless, by varying the photon energy and the tunnel barrier thickness, it is possible to filter out the magneto-optical effects. Using this procedure, we have obtained some experimental evidence for the presence of spin-polarized tunnelling by optical spin orientation in $Co/Al_2O_3/GaAs$ junctions, where the deduced relative spin-splitting at the semiconductor surface $([V_s^\uparrow - V_s^\downarrow]/[V_s^\uparrow + V_s^\downarrow])$ amounts to 5×10^{-2} or less. In MBE-grown samples with an AlAs barrier we did not observe spin-polarized tunnelling, most probably due to the presence of an ultrathin τ-MnAl layer adjacent to the AlAs barrier. The ultrathin template was needed for high-quality Co epitaxy. Spin-split bandstructure calculations confirmed that the conductance along the tunnelling direction is hardly spin polarized due to the τ-MnAl layer.

For future experiments it is important to reduce the magneto-optical contribution to the tunnel current modulation. Since the Faraday effect scales with the film thickness, ultrathin magnetic films can be used, such as MBE-grown Fe or Co (e.g. [58, 59]). Also it is of interest to avoid the appearance of low-resistance spots in the devices, for example by edge passivation; this will allow for detailed studies of the current–voltage characteristics, and for studies of the voltage dependence of the spin-polarized tunnelling current.

Finally, we discuss the consequences of the previous model description and experimental results for the development of a convenient magnetically sensitive probe material in an STM. As was pointed out in the introductory section of this paper, for a spin-sensitive material there are essentially three possibilities: a superconductor, a magnetic material, or a semiconductor.

(i) *Superconductor.* The application of a superconductor for spin-polarized tunnelling in an STM is difficult, because a tip with a superconducting state at the apex has to be operated in rather high magnetic fields. To our knowledge, this technique has not yet been applied in an STM.

(ii) *Magnetic material.* Due to magnetostriction and magnetostatic interactions, in an STM the relative orientation of the tip and sample magnetization is not easily modified without changing the tip-to-sample distance. In addition, the perturbation of the sample magnetic structure by the tip remains a matter of concern. It may, however, be possible to obtain some information on spin-polarized tunnelling by comparing the surface topography and current–voltage characteristics measured with a magnetic tip on different atomic sites.

(iii) *Semiconductor.* The advantage of a photoexcited semiconductor probe is that the spin orientation can be modified by optical means. Pioneering STM tests of spin-polarized tunnelling with GaAs are being performed [60, 61], where it is essential to separate the spin-selective and spin-integrated contributions to the tunnelling current (cf. equation (5)). In a metal–semiconductor STM junction there is a strong voltage dependence of the sensitivity of the current to variations of the optical power [24]; thus by sweeping the voltage, we can tune the tunnel junction to a low sensitivity to variations of the optical power, in order to isolate a signal due to spin-polarized tunnelling. The dual-frequency modulation technique involved and experimental results are presented in [61].

Also, it is of interest to estimate the importance of magnetic forces when photoexcited GaAs is used in an STM. For 1.5 eV photons the absorption depth is about 1 μm in GaAs [62]; if every photon yields one electron–hole pair, for an excitation intensity of 10^7 W m^{-2} the photoelectron generation rate is 4×10^{31} electrons per second per m^3. In the case of 50% spin polarization and a lifetime of 10 ns, in the semiconductor this gives a maximum photoinduced magnetization of 2×10^{23} μ_B m^{-3}. This is equal to an average optically induced magnetic moment of less than 10^{-5} μ_B per atom. With such a low magnetization the resulting magnetic dipolar forces are negligibly small. It is more difficult to evaluate the size of an exchange force in an optically oriented metal–semiconductor tunnel junction, because of the nonequilibrium spin dynamics involved. Although a spin-splitting as high as 0.1 V may be achievable, this is still an order of magnitude smaller than the exchange splitting in Fe or Co. From the above estimates we conclude that the magnetic forces in a tunnel junction between a ferromagnetic material and an optically excited semiconductor are small compared to the case for two magnetic counter-electrodes.

Acknowledgments

We thank J Hermsen, J Gerritsen and A van Etteger for technical support. M Stoelinga performed calibration measurements. A van Geelen kindly supplied us with semiconductor materials. We thank H Salemink for critically reading the manuscript. Part of this work was supported by the Stichting Fundamenteel Onderzoek der Materie (FOM), which is financially supported by the Nederlandse Organisatie voor Wetenschappelijk Onderzoek (NWO). WVR acknowledges support as a Research Assistant of the National Fund for Scientific Research (Belgium).

References

[1] Meservey R and Tedrow P M 1994 *Phys. Rep.* **238** 173

[2] A review on STM can be found in
Wiesendanger R and Güntherodt H-J (ed) 1992/93 *Scanning Tunnelling Microscopy I, II and III (Springer Series in Surface Science 20, 28 and 29)* (Heidelberg: Springer)

[3] Slonczewski J C 1989 *Phys. Rev.* **39** 6995
Minakov A A and Shvets I V 1990 *Surf. Sci. Lett.* **236** L377
Molotkov S N 1992 *Surf. Sci.* **261** 7
Bürgler D and Tarrach G 1992 *Ultramicroscopy* **42** 194

[4] Moodera J S, Kinder L R, Wong T M and Meservey R 1995 *Phys. Rev. Lett.* **74** 3273
Miyazaki T and Tezuka N 1995 *J. Magn. Magn. Mater.* **139** L231 and references therein

[5] Wiesendanger R, Güntherodt H-J, Güntherodt G, Gambino R J and Ruf R 1990 *Phys. Rev. Lett.* **65** 247

[6] Alvarado S F and Renaud P 1992 *Phys. Rev. Lett.* **68** 1387

[7] Meier F and Zakharchenya B P (ed) 1984 *Optical Orientation (Modern Problems in Condensed Matter Sciences 8)* (Amsterdam: Elsevier)

[8] *Japanese Patent* A62139240 (Hitachi Ltd), publication date 22 June 1987
European Patent A0355241 (IBM Corporation), publication date 28 February 1990

[9] Pierce D T 1988 *Phys. Scr.* **38** 291

[10] Wolters W T M 1988 *Master's Thesis* University of Nijmegen

[11] Molotkov S N 1992 *JETP Lett.* **55** 174

[12] Laiho R and Reittu H J 1993 *Surf. Sci.* **289** 363

[13] Reittu H J 1994 *J. Phys.: Condens. Matter* **6** 1847

[14] Hermann C, Drouhin H-J, Lampel G, Lassailly Y, Paget D, Peretti J, Houdré R, Ciccacci F and Riechert H 1992 *Spectroscopy of Nonequilibrium Electrons and Phonons* ed C V Shank and B P Zakharchenya (Amsterdam: Elsevier) ch 9, p 397

[15] Prins M W J, Abraham D L and Van Kempen H 1993 *J. Magn. Magn. Mater.* **121** 109; 1993 *Surf. Sci.* **287/288** 750

[16] Nunes G and Amer N M 1993 *Appl. Phys. Lett.* **63** 1851

[17] Prins M W J, Van Der Wielen M C M M, Jansen R, Abraham D L and Van Kempen H 1994 *Appl. Phys. Lett.* **64** 1207

[18] Jansen R, Van Der Wielen M C M M, Prins M W J, Abraham D L and Van Kempen H 1994 *J. Vac. Sci. Technol.* B **12** 2133

[19] Lang N D 1993 *Scanning Tunnelling Microscopy III (Springer Series in Surface Science 29)* ed R Wiesendanger and H-J Güntherodt (Heidelberg: Springer)

[20] Pierce D T and Celotta R J 1984 *Optical Orientation (Modern Problems in Condensed Matter Sciences 8)* ed F Meier and B P Zakharchenya (Amsterdam: Elsevier) ch 6

[21] The electron energy and spin relaxation are very efficient in a magnetic metal. This implies that a tunnelling experiment is insensitive in principle to the details of carrier relaxation in the magnetic material. In contrast, experiments on actual electron transmission through a magnetic thin film are sensitive to the spin dependence of the carrier relaxation. See, for example,
Lassailly Y, Drouhin H-J, Van Der Sluis A J, Lampel G and Marlière C 1994 *Phys. Rev.* B **50** 13 054
Gröbli J C, Guarisco D, Frank S and Meier F 1995 *Phys. Rev.* B **51** 2945
Monsma D J, Lodder J C, Popma Th J A and Dieny B 1995 *Phys. Rev. Lett.* **74** 5260

[22] Ahrenkiel R K 1993 *Minority Carriers in III–V Semiconductors: Physics and Applications (Semiconductors and Semimetals 39)* ed R K Ahrenkiel and M S Lundstrom (San Diego, CA: Academic) ch 2, p 39

[23] A modulation of optical power causes a nonzero $\Delta\overline{V_s}$, but also affects the value of ΔV_s^{spin}. However, the relative change of the value of ΔV_s^{spin} is only of the order of $\Delta\overline{V_s}/\overline{V_s}$, which is negligible in our experiments.

[24] Prins M W J, Jansen R, Groeneveld R H M, van Gelder A P and Van Kempen H 1995 Photoelectrical properties of semiconductor tips in scanning tunnelling microscopy, submitted
Prins M W J 1995 *PhD Thesis* University of Nijmegen

[25] Note that in a semiconducting material it is important to discriminate between majority and minority *carriers* (holes or electrons). In magnetic materials it is often useful to distinguish the majority and minority *spin direction*. The notions of majority and minority particles always refer to the situation encountered in the bulk of the material.

[26] Wieder H H 1980 *J. Vac. Sci. Technol.* **17** 1009 and other contributions in that issue

[27] Dyakonov M I and Perel V I 1984 *Optical Orientation (Modern Problems in Condensed Matter Sciences 8)*

ed F Meier and B P Zakharchenya (Amsterdam: Elsevier) ch 2

[28] In n-type GaAs, the optically oriented electrons (now the majority carriers) are swept into the semiconductor bulk by the subsurface electric field. Hence, in principle the semiconductor surface can become spin polarized by *majority-carrier* transport over the Schottky barrier.

[29] Rhoderick E H and Williams R H 1988 *Metal–Semiconductor Contacts (Monographs in Electrical and Electronic Engineering 19)* (Oxford: Clarendon)

[30] Sze M S 1981 *Physics of Semiconductor Devices* (New York: Wiley)

[31] For a review on magneto-optical effects see:
Freiser M J *IEEE Trans. Magn.* **MAG-4** 152

[32] To first order, the contributions to the helicity asymmetry of the tunnel current from spin-polarized tunnelling and from the magneto-optical effect depend linearly on the product of the light helicity and the sample magnetization. As a result, these two contributions cannot be separated by modifying the optical polarization or the sample magnetization.

[33] Woodruff D P and Delchar T A 1986 *Modern Techniques of Surface Science* (London: Cambridge University Press)

[34] Koch A J J, Hokkeling P, Van Der Steeg M G and De Vos K J 1960 *J. Appl. Phys.* **31S** 75S

[35] Sands T, Harbison J P, Leadbeater M L, Allen J S J, Hull G W, Ramesh R and Keramidas V G 1990 *Appl. Phys. Lett.* **57** 2609

[36] Prinz G A 1985 *Phys. Rev. Lett.* **54** 1051

[37] Liu A Y and Singh D J 1993 *J. Appl. Phys.* **73** 6189

[38] De Boeck J, Bruynseraede C, Bender H, Van Esch A, Van Roy W and Borghs G 1995 *J. Cryst. Growth.* **150** 1139

[39] Hunt R P 1967 *J. Appl. Phys.* **38** 1652
Atkinson R and Lissberger P H 1993 *J. Magn. Magn. Mater.* **118** 271

[40] Reim W and Schoenes J 1990 *Ferromagnetic Materials* vol 5, ed K H J Buschow and E P Wohlfarth (Amsterdam: Elsevier) p 134

[41] Van Engen P G, Buschow K H J and Erman M 1983 *J. Magn. Magn. Mater.* **30** 374

[42] Johnson P B and Christy R W 1972 *Phys. Rev.* B **6** 4370; 1974 *Phys. Rev.* B **9** 5056

[43] Pierce D T and Meier F 1976 *Phys. Rev.* B **13** 5484

[44] Drouhin H-J, Hermann C and Lampel G 1985 *Phys. Rev.* B **31** 3872

[45] Wolf E L 1985 *Principles of Electron Tunnelling Spectroscopy* (New York: Oxford University Press)

[46] We neglected the spin-selective contribution with respect to the spin-integrated contribution. This is permissible, because we will find that the relative spin-splitting at the semiconductor surface was far smaller than unity in this experiment.

[47] Kessler J 1976 *Polarized Electrons (Springer Series on Atoms and Plasmas 1)* (Berlin: Springer)

[48] In the convention described in [40], for Co and using radiation with a photon energy between 1.5 and 3 eV, the polar Kerr rotation and ellipticity are negative and the Faraday rotation and ellipticity are positive—see, for example,
Clemens K H and Jaumann J 1963 *Z. Phys.* **173** 135
or [41]. When the magnetic field is oriented in the propagation direction of the incident beam, this means that incident light of right-handed circular polarization is absorbed more strongly than light of left-handed circular polarization, where right- (left-) handed circular polarization means that at a fixed location the electric vector rotates clockwise (anticlockwise) for an observer facing the optical beam. The radiation *helicity* is defined as the angular momentum with respect to a fixed quantization axis. If the quantization axis is defined as *opposite* to the propagation direction of the light, right- (left-) handed circularly polarized light is of positive (negative) helicity.

[49] Weber W, Wesner D A, Hartmann D and Güntherodt G 1992 *Phys. Rev.* B **46** 6199

[50] Carbone C, Vescovo E, Rader O, Gudat W and Eberhardt W 1993 *Phys. Rev. Lett.* **71** 2805

[51] τ-MnAl has a tetragonal crystal structure with $a = 2.77$ Å and $c = 3.54$ Å (space group 123 in the *International Tables* [52]). The Wyckoff positions a and d are occupied. The ratio of Mn to Al was taken to be 50/50. *Ab initio* localized-spherical-wave (LSW) bandstructure calculations [53] were performed using a scalar-relativistic Hamiltonian and including all core electrons. Local-density exchange–correlation potentials [54] inside space-filling, and therefore overlapping, spheres around the atomic constituents were used. In the construction of the LSW basis [53], the spherical waves were augmented by solutions of the scalar-relativistic radial equations indicated by the atomic-like symbols 3s and 3p for Al and 4s, 4p and 3d for Mn. In the internal l-summation for the augmentation of the central Hankel function at surrounding atomic sites one extra l-value was included, i.e. 3d orbitals were added on Al and 4f orbitals on Mn. About 150 degrees of freedom were used for screening the central Hankel functions, resulting in screening

clusters with a size of 27 atoms. Iterations were performed with k-points lying in the centres of simplexes filling an irreducible part of the first Brillouin zone. The volume per point was 2.6×10^{-7} Å^{-3}. Self-consistency was assumed when the changes in the local partial charges in each atomic sphere decreased to below 10^{-4}. Subsequently the densities of states were obtained by an analytical quadratic integration method [55] using the k-points on the apices and mid-vertices of the simplexes.

[52] Hahn T (ed) 1983 *Space Group Symmetry (International Tables for Crystallography vol A)* (Dordrecht: Reidel)

[53] Van Leuken H, Lodder A, Czyżyk M T, Springelkamp F and De Groot R A 1990 *Phys. Rev.* B **41** 5613

[54] Hedin L and Lundqvist B I 1971 *J. Phys. C: Solid State Phys.* **4** 2064

[55] Methfessel M S, Boon M H and Muller F M 1987 *J. Phys. C: Solid State Phys.* **20** 1069

[56] The tunnelling through a planar barrier is direction sensitive because an electron with a large momentum parallel to the tunnel barrier (and so with a large transverse kinetic energy) has a low penetration into the tunnelling barrier [57]. Assume an electron with a wavevector that is at an angle α with respect to the sample normal; by simple plane-wave matching, it can easily be derived that the relative transmission probability through the tunnel barrier is given by: $T(\alpha)/T(\alpha = 0) = \exp(-2d\,\Delta\kappa)$, where $\Delta\kappa$ equals $k^2\alpha^2/[2\kappa]$ to lowest order in α; d is the tunnel barrier width and k is the wavevector of the impinging electron; for a square barrier κ is equal to $[2m\Phi_t/\hbar^2]^{1/2}$, where Φ_t is the tunnel barrier height. Our experiment involves an AlAs barrier with a thickness (d) of 20 nm. AlAs has an energy gap of more than 2 eV, such that a tunnel barrier height (Φ_t) of 1 eV is a reasonable value; this yields $\kappa = 5.2$ nm^{-1}. Assuming a wavevector $k = 10$ nm^{-1} for the impinging electron, we find that the relative transmission drops by a factor of ten for an angle of incidence (α) of 5°. This estimate is in agreement with the calculations of [57].

[57] Beuermann G 1981 *Z. Phys.* B **44** 29

[58] Anderson G W, Hanf M C and Norton P R 1995 *Phys. Rev. Lett.* **74** 2764
Prinz G A 1990 *Science* **250** 1092

[59] Moghadam A, Booth J G, Lord D G, Boyle J and Boardman A D 1994 *IEEE Trans. Magn.* **MAG-30** 769 and references therein

[60] Sueoka K, Mukasa K and Hayakawa K 1993 *Japan. J. Appl. Phys.* **32** 2989

[61] Prins M W J, Jansen R and Van Kempen H 1995 Spin-polarized tunnelling with GaAs tips in scanning tunnelling microscopy, submitted
Prins M W J 1995 *PhD Thesis* University of Nijmegen

[62] Aspnes D E and Studna A A 1983 *Phys. Rev.* B **27** 985